



Secondary ozone peaks in the troposphere over the Himalayas

Narendra Ojha¹, Andrea Pozzer¹, Dimitris Akritidis^{1,2}, and Jos Lelieveld^{1,3}

¹Atmospheric Chemistry Department, Max Planck Institute for Chemistry, Mainz, Germany

²Department of Meteorology and Climatology, School of Geology, Aristotle University of Thessaloniki, Thessaloniki, Greece

³Energy, Environment and Water Research Center, The Cyprus Institute, Nicosia, Cyprus

Correspondence to: Narendra Ojha (narendra.ojha@mpic.de)

Received: 10 October 2016 – Discussion started: 2 November 2016

Revised: 25 March 2017 – Accepted: 5 May 2017 – Published: 8 June 2017

Abstract. Layers with strongly enhanced ozone concentrations in the middle–upper troposphere, referred to as secondary ozone peaks (SOPs), have been observed in different regions of the world. Here we use the global ECHAM5/MESSy atmospheric chemistry model (EMAC) to (i) investigate the processes causing SOPs, (ii) explore both their frequency of occurrence and seasonality, and (iii) assess their effects on the tropospheric ozone budget over the Himalayas. The vertical profiles of potential vorticity (PV) and a stratospheric ozone tracer (O_3S) in EMAC simulations, in conjunction with the structure of SOPs, suggest that SOPs over the Himalayas are formed by stratosphere-to-troposphere transport (STT) of ozone. The spatial distribution of O_3S further shows that such effects are in general most pronounced in the northern part of India. Model simulated ozone distributions and backward air trajectories show that ozone rich air masses, associated with STT, originate as far as northern Africa and the North Atlantic Ocean, the Middle East, as well as in nearby regions in Afghanistan and Pakistan, and are rapidly (within 2–3 days) transported to the Himalayas. Analysis of a 15-year (2000–2014) EMAC simulation shows that the frequency of SOPs is highest during the pre-monsoon season (e.g. 11 % of the time in May), while no intense SOP events are found during the July–October period. The SOPs are estimated to enhance the tropospheric column ozone (TCO) over the central Himalayas by up to 21 %.

1 Introduction

Tropospheric ozone is a short-lived climate forcer (Shindell et al., 2012) and an air pollutant with adverse effects on human health and crop yields (Monks et al., 2015, and references therein). The effects of tropospheric ozone on crop yields and human health occur near the surface, whereas its radiative forcing is shown to be strongest in the middle–upper troposphere (e.g. Lacis et al., 1990; Myhre et al., 2013; Monks et al., 2015). The processes controlling tropospheric ozone in the middle and upper troposphere can be different from those near the surface. The photochemistry, involving non-methane volatile organic compounds (NMVOCs) and carbon monoxide in the presence of nitrogen oxides (NO_x), primarily controls ozone pollution in the planetary boundary layer. In contrast, dynamics involving stratosphere–troposphere exchange (STE) play a key role in the middle–upper troposphere (e.g. Holton and Lelieveld, 1996; Lelieveld and Dentener, 2000; Neu et al., 2014; Ojha et al., 2014; Monks et al., 2015). Therefore, to quantify the relative contributions of photochemical and dynamical processes to the ozone budget and assess the climatic impacts of anthropogenic ozone, studies on the vertical distribution of ozone are essential.

Ozone observations have been conducted globally and locally using different instruments and platforms as reviewed recently by Tanimoto et al. (2015). Balloon-borne observations employing ozone-sondes offer the advantage of measuring ozone across the tropopause. Analyses of ozone-sonde observations have provided valuable information on the variability, general features and trends in ozone profiles (e.g. Logan, 1985, 1994). Secondary maxima in ozone profiles, called secondary ozone peaks (SOPs), are a unique phe-

nomenon in which anomalously large ozone concentrations are observed in confined layers in the middle–upper troposphere or lower stratosphere.

The occurrences of SOPs, underlying processes and their global distribution have been discussed in a limited number of studies (Dobson, 1973; Reid and Vaughan, 1991; Varotsos et al., 1994), reviewed by Lemoine (2004). SOPs have been commonly observed at high latitudes, for example, as laminated structures of ozone with the highest frequency of occurrence during the spring season (Dobson, 1973). These laminated structures are primarily considered to be a winter–spring phenomenon, with a peak altitude of occurrence near 14 km (Reid and Vaughan, 1991). Varotsos et al. (1994) suggested that the northern and north-western atmospheric circulations in the lower stratosphere play a key role in the formation of SOPs observed over Athens, Greece. Overall, the occurrence of SOPs is typically considered to be a Northern Hemispheric phenomenon, with no SOPs reported in the tropics and the Southern Hemisphere (Lemoine, 2004). Trickl et al. (2011) showed the influences of ozone import from the stratosphere and transport along the subtropical jet stream over Europe. According to the aforementioned studies, SOPs are mainly attributed to dynamical processes involving STE, advection and Rossby wave breaking events.

Recent studies (Hwang et al., 2005, 2007; Park et al., 2012) focusing on the Korean region showed that SOP events regularly occur over midlatitudes. In contrast to earlier studies that demonstrated the occurrence of SOPs mostly in the lower stratosphere, several SOPs were observed in the upper troposphere over Korea. Hwang et al. (2005) attributed these SOPs to the downward transport of ozone from the stratosphere on a timescale of about 1 day (24 h), typical of cross-tropopause exchange. Furthermore, the frequency of occurrence, estimated from 9 years of ozone-sonde observations, was found to have strong seasonal variability over Korea with a broad winter–spring maxima and frequencies of occurrence up to 50–80 % (Hwang et al., 2005). Moreover, Hwang et al. (2005) reported an increase in SOP occurrences over Korea, while the STT effects are anticipated to increase tropospheric ozone in the future (Banerjee et al., 2016).

The studies pertaining to the influences of STT on the vertical profiles of ozone are relatively sparse over the tropical Indian region. Mandal et al. (1998) analysed observations from ozone-sondes and an MST radar, and attributed the enhanced ozone mixing ratios in the upper troposphere to STT through the indistinct tropopause over southern India. Fadnavis et al. (2010) combined satellite-borne measurements (TES and MLS) with simulations performed by the MOZART model and showed significant influences of STT over India, in particular during winter and spring/premonsoon. Venkat Ratnam et al. (2016) used satellite observations to estimate the effect of STE associated with tropical cyclones over the northern Indian Ocean. Most of the studies based on in situ measurements have, however, been confined to the southern part of India (e.g. Mandal et al., 1998;

Sinha et al., 2016) and the adjacent marine regions (Lal et al., 2013). Ganguly and Tzanis (2011) used ozone-sonde observations from three Indian stations operated by the Indian Meteorological Department (IMD) and suggested that overall STT only plays a minor role in the budget of tropospheric ozone over India. However, the influences of STT were found to increase with latitude/northward over India (Ganguly and Tzanis, 2011).

Studies investigating the SOP structures and implications have been few over the tropical Indian region until very recently (Ojha et al., 2014; Das et al., 2016). The events over southern India were found to be mainly associated with stratospheric intrusions during tropical cyclonic storms (Das et al., 2016). In contrast, the SOP events observed over the central Himalayas in northern India appear to be similar to what is typically observed over the middle–high latitudes as mentioned earlier. Moreover, SOPs were observed to be more frequent during spring, and were attributed to the combined effects of STE and advection (Ojha et al., 2014). In the previous work using weekly ozone-sonde measurements (3–4 profiles per month), covering the period January 2011–December 2011 (Ojha et al., 2014), only six SOP events were observed, being insufficient to calculate the frequency and seasonality of SOP occurrences. Additionally, model simulations are required to both trace the source regions and quantify the effect of SOPs on the tropospheric ozone budget. Such investigations are of key importance as the Indo-Gangetic Plain (IGP) and Himalaya region are global hotspot regions in terms of anthropogenic pressures that could impose threats to Asia's water and food security (Ramanathan et al., 2008). Satellite-based studies corroborate the high pollution loading over northern India and the nearby IGP including the tropospheric column ozone (TCO) over South Asia (Fishman et al., 2003). The IGP is a regional hotspot for atmospheric brown clouds (ABCs), consisting of brown haze formed by submicron size aerosol particles and emitted from a wide range of anthropogenic and natural sources. It has been shown that ABCs reduce the amount of sunlight that reaches the Earth's surface by as much as 10 to 15 % and enhance atmospheric solar heating by as much as 50 % (Ramanathan et al., 2007).

In the present study, the global atmospheric chemistry climate model EMAC (ECHAM5/MESSy Atmospheric Chemistry) has been used to explore the processes causing the SOPs, investigate the frequency and seasonality of their occurrence and finally assess their impact on the tropospheric ozone budget over the central Himalayas.

2 Methodology

2.1 EMAC

The ECHAM5/MESSy Atmospheric Chemistry (EMAC) is a numerical system for the simulation of regional and global

air quality and climate (Jöckel et al., 2010). In this work the model results from simulation RC1SD-base-10a of the ESCiMo project (Jöckel et al., 2016) are used. The general circulation model ECHAM5 version 5.3.02 (Roeckner et al., 2006) and the Modular Earth Submodel System (MESSy) version 2.51 (Jöckel et al., 2016) were used at T42L90MA resolution, implying a spherical truncation of T42 (corresponding to a quadratic Gaussian grid of approx. 2.8 by 2.8° in latitude and longitude) and 90 vertical hybrid pressure levels up to 0.01 hPa. The dynamics of the general circulation model were weakly nudged by Newtonian relaxation towards ERA-Interim reanalysis data (Dee et al., 2011). Gas-phase and particulate trace species calculated with the EMAC model have been extensively evaluated in previous studies (e.g. Pozzer et al., 2007, 2010, 2012). Simulation RC1SD-base-10a with model output every 10 h, was selected between the ESCiMo simulations as suggested in Jöckel et al. (2016): “For intercomparison with observations, we recommend to use the results of [...] RC1SD-base-10a.”. Detailed information on the model set-up and comparison with observations can be found in Jöckel et al. (2016).

A tracer of stratospheric ozone, denoted by O_3s in EMAC, has been used to quantify the effects of STT. O_3s follows the transport and destruction processes of ozone in the troposphere but not its chemical formation (Roelofs and Lelieveld, 1997) and it is initialized to O_3 in the stratosphere.

2.2 Tropopause height and tropopause folds

The lapse rate tropopause (LRT) height is calculated from EMAC output using the WMO definition as the altitude at which lapse rate decreases to a value of 2 °C km^{-1} or less, provided that the average lapse rate between this level and all higher levels within the adjacent 2 km does not exceed 2 °C km^{-1} .

Tropopause folds in EMAC simulations were identified with an algorithm developed by Sprenger et al. (2003), and improved by Škerlak et al. (2014) using the three dimensional fields of potential vorticity, potential temperature and specific humidity. The vertical extent of the folds, as determined by the difference between the upper and mid-tropopause crossings (see Fig. 1 in Tyrlis et al., 2014) has been further used to identify shallow, medium and deep folds, as described and used elsewhere (Tyrlis et al., 2014; Škerlak et al., 2015; Akritidis et al., 2016).

2.3 Observational data set

The occurrence of SOPs was reported using ozone-sonde observations from Nainital (79.45° E , 29.37° N , 1958 m a.s.l.), a high altitude station located in the central Himalayan region (Fig. 1; Ojha et al., 2014). These data have been used to evaluate the capability of EMAC to reproduce SOPs over this region. Some typical events of SOP occurrence over Nainital can be seen in Fig. 2. The ozone mixing ratios in the

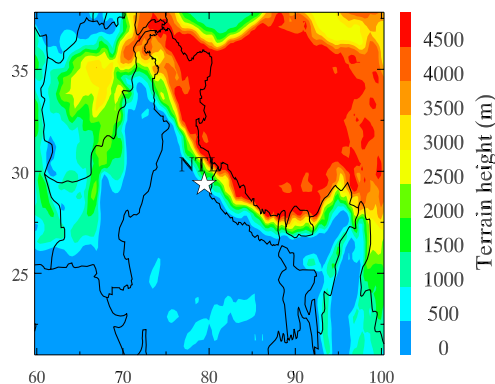


Figure 1. Location of the Nainital site in the central Himalayas shown on the topography map of the northern Indian region.

mid-troposphere (10–11 km) are clearly observed to be very high ($150\text{--}250\text{ nmol mol}^{-1}$) forming an SOP. The location of Nainital station and the geographical topography of the northern Indian region are also shown in Fig. 1.

Ozone profiles at Nainital were measured using electrochemical concentration cell (ECC) ozone-sondes. The method utilizes the titration of ozone in potassium iodide solution, which leads to the production of iodine (I_2). The conversion of I_2 to I^- in the cell leads to the flow of two electrons for each ozone molecule entered. The measured cell current and flow rate of air along with sensor parameters, e.g. the background current and pump temperature, are used to derive ozone mixing ratios (Ojha et al., 2014). The precision and accuracy of ECC ozone-sondes are reported to be $\pm(3\text{--}5)\%$ and $\pm(5\text{--}10)\%$ respectively, up to 30 km altitude (Smit et al., 2007).

The year-long observations analysed previously (Ojha et al., 2014) showed six occurrences of elevated ozone layers in the 10–12 km altitude range, identified as SOPs. For the analysis of frequency of occurrence and impacts of SOPs, we classify an ozone profile as SOP if (1) O_3 mixing ratios at 10–12 km are higher by at least by 50 % compared to average ozone in the lower troposphere and (2) O_3 mixing ratios are again lower (at least by 20 %) above the SOP (as shown in Fig. 2 and described in more detail in the Sect. 3.3).

Further details of the Nainital station and meteorology (Sarangi et al., 2014; Singh et al., 2016) and balloon-borne measurements (Smit et al., 2007; Ojha et al., 2014; Naja et al., 2016) can be found elsewhere.

2.4 Backward trajectories

We used the Hybrid Single Particle Lagrangian Integrated Trajectory (HYSPLIT) model (<http://ready.arl.noaa.gov/HYSPLIT.php>) to investigate the source regions and the transport patterns causing SOPs over the central Himalayas. Five-day backward trajectories have been simulated at 10, 11 and 12 km above sea level (a.s.l.) (Fig. S4 in the Supple-

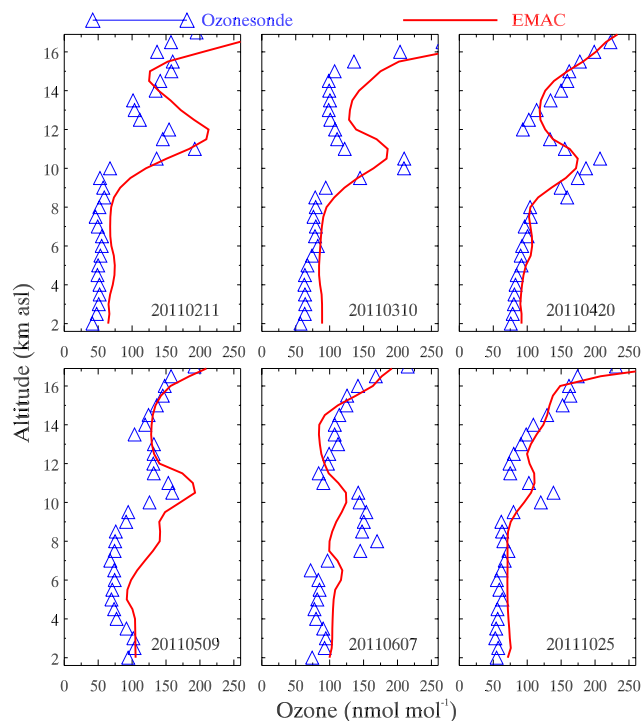


Figure 2. Comparison of EMAC-simulated ozone profiles during the days of SOP events with ozone-sonde observations over Nainital.

ment), which are the typical altitudes for the six SOP events shown in Fig. 2. Additional trajectories have been computed for each model time step in the month of May 2002 (Fig. 6), during which the model predicts the highest frequency of occurrence in the 2000–2014 period. HYSPLIT trajectory simulations are driven by NCEP reanalysis meteorological fields and the model vertical velocity option has been used for the vertical motions. More details of the backward trajectory simulations using the HYSPLIT model (Draxler and Hess, 1997, 1998; Draxler et al., 2014) and use of various data sets as meteorological inputs over the Indian region can be found elsewhere (e.g. Ojha et al., 2012; Kumar et al., 2015).

3 Results and discussion

3.1 Model evaluation

Figure 2 shows the comparison of EMAC-simulated ozone profiles with ozone-sonde measurements over Nainital during six SOP events reported previously (Ojha et al., 2014). Model ozone fields have been bilinearly interpolated to the observation site, and model output closer to the time of observation is weighted higher (Ojha et al., 2016). As the vertical resolution of EMAC simulations is about 500–600 m in the mid-troposphere (10–12 km), where SOPs are typically observed, the observational values are also shown at similar

vertical resolution for comparison. The average ozone mixing ratios along with the corresponding standard deviations for the six events are compared between the model and observations in Table 1 for lower-, middle- and upper-tropospheric altitudes.

The EMAC model is found capable of reproducing the altitudinal placement of the SOPs over the central Himalayas during all six events. For example, on 20 April and 9 May the model shows the peak ozone mixing ratios at 10.5 km a.s.l., in agreement with the ozone-sonde profiles. On other days, such as on 11 February, 10 March and 25 October, the altitude of SOP differs slightly (by 0.5–1 km) between the model and ozone-sonde profiles, except on 7 June (by 2 km). The aforementioned discrepancies in the altitude of SOPs occurrence might be related to the model vertical resolution.

In addition to the altitude of SOPs occurrence, EMAC also quantitatively captures the ozone enhancements. The model bias in simulating peak ozone mixing ratios is found to vary from about -26% (7 June) to $+21\%$ (9 May). The biases are found to be within the variability of 1 standard deviation in 10–12 km altitude ($28\text{--}59\text{ nmol mol}^{-1}$) as calculated from ozone-sonde observations during spring over this site (see Table 1 and Ojha et al., 2014).

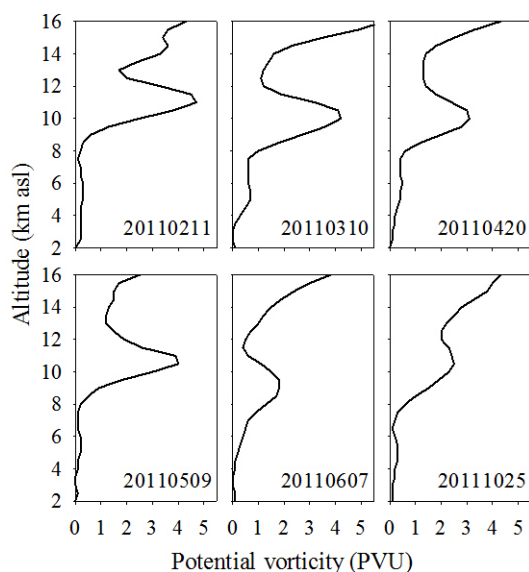
However, the model generally overestimates the ozone mixing ratios in the lower troposphere by about $11\text{--}24\text{ nmol mol}^{-1}$ (Table 1) and shows some limitation in capturing less pronounced SOPs, typically observed outside the winter–spring seasons. The bias in the absolute ozone enhancement (-45 nmol mol^{-1}) as well as in the altitudinal placement of the SOP (by 2 km) is higher on 7 June. Here EMAC simulations are evaluated for all events identified visually (Ojha et al., 2014). The SOP events are selected based on specific criteria in order to calculate the frequency of occurrence, as discussed in detail in Sect. 3.3.

Possible biases between the model and observations could arise from a variety of sources, most importantly, the time evolution of the SOPs (Supplement, Fig. S1). Therefore, the limited number of ozone profile measurements could lead to a temporal difference in the state of SOP evolution being compared between the model and the observation. We tried to minimize this effect by applying a weighted-average algorithm, as mentioned above.

Overall, the model is found to be able of reproducing the occurrence of SOPs, their altitudinal placements and the ozone enhancements over the central Himalayas. Additionally, EMAC-simulated average ozone distribution appears to compare well with the ozone-sonde climatology over Delhi (77.16° E , 28.49° N) in northern India (Fig. S2) and with aircraft-based measurements from the IAGOS-CARIBIC programme (Jöckel et al., 2016). Hence, we use the EMAC simulations to investigate the underlying processes (Sect. 3.2), the frequency of occurrences (Sect. 3.3) and the effects on tropospheric ozone budget (Sect. 3.4).

Table 1. A comparison of average ozone mixing ratios between ozone-sondes and EMAC model for the lower, middle and upper troposphere during the six SOP events over Nainital.

Date dd/mm/yyyy	2–7 km		7–12 km		12–17 km	
	Sonde	EMAC	Sonde	EMAC	Sonde	EMAC
11/02/2011	50.7 ± 4.1	69.5 ± 3.6	85.8 ± 52.1	112.3 ± 52.3	135.9 ± 22.9	173.7 ± 42.6
10/03/2011	67.6 ± 8.1	86.8 ± 1.8	120.5 ± 52.0	134.8 ± 39.0	131.9 ± 57.4	184.7 ± 76.9
20/04/2011	85.8 ± 7.7	96.9 ± 7.0	147.1 ± 37.3	136.8 ± 28.6	151.4 ± 41.6	151.0 ± 36.7
09/05/2011	83.0 ± 13.3	101.6 ± 5.3	104.8 ± 34.7	154.8 ± 25.3	132.9 ± 15.4	140.7 ± 17.7
07/06/2011	83.1 ± 7.6	107.0 ± 6.1	132.4 ± 30.2	110.2 ± 10.0	119.8 ± 21.6	111.9 ± 35.2
25/10/2011	57.1 ± 3.3	72.3 ± 1.7	84.4 ± 26.8	86.7 ± 17.2	123.3 ± 37.6	130.4 ± 31.7

**Figure 3.** Vertical profiles of potential vorticity (PV) from EMAC simulations during the SOPs over Nainital.

3.2 Origin of SOPs

In this section, we analyse the EMAC-simulated meteorological and chemical fields in conjunction with backward air trajectories to investigate the origin of SOPs over the central Himalayas. Figure 3 shows the vertical profiles of potential vorticity (PV), a tracer of stratospheric intrusions, during the SOP events observed over Nainital. PV vertical profiles during all SOPs show layers of high values coinciding with the altitude of SOPs.

The enhanced PV layers are found to be weaker during June and October compared to events during late winter and spring. PV values are found to be between 3.1 PVU (20 April) and 4.7 PVU (11 February) at the SOP altitudes for the events occurring in winter–spring. Even during the less pronounced events of early summer and autumn, the PV values at SOP altitude are 1.8–2.5 PVU. Further, the average vertical profile of PV during SOPs, derived from a long-term model simulation (2000–2014), shows a

similar structure (Supplement, Fig. S3), as shown here for the individual events. Average PV values during SOPs are found to be significantly higher (e.g. 3.0 ± 1.3 PVU in winter, 1.8 ± 0.5 PVU during summer monsoon) compared to time steps without SOP (0.3 ± 0.2 – 1.5 ± 1.3 PVU) (Supplement, Table S1). Such enhanced PV values during the SOPs suggest that the air masses showing very high ozone levels (SOPs) are of stratospheric origin.

To quantify the amount of ozone transported from the stratosphere during the SOPs, we compare the EMAC-simulated vertical profiles of O_3 with O_{3s} during six observed SOP events (Fig. 4). O_{3s} values are very similar to O_3 indicating that nearly all the excess ozone that constitutes SOPs is of the stratospheric origin, except on 7 June and 25 October. The contribution of tropospheric photochemical sources to the SOPs, as represented by the difference $O_3 - O_{3s}$, is found to be significant on 25 October (15 nmol mol^{-1}) and is much larger on 7 June (50 nmol mol^{-1}).

The comparison of O_3 with O_{3s} is further analysed for the extended period 2000–2014 and a seasonal climatology is derived by aggregating all SOP events into four different seasons (Fig. 5). The average amount of ozone transported from the stratosphere to the SOPs is found to be the highest during spring ($162.5 \pm 40 \text{ nmol mol}^{-1}$), followed by winter ($149.4 \pm 35 \text{ nmol mol}^{-1}$). In contrast the contribution of tropospheric photochemical sources to the SOPs is highest during the summer monsoon (30 nmol mol^{-1}). The stronger contribution of tropospheric photochemical O_3 up to (and beyond) the SOP altitudes during the summer monsoon could be a combined effect of deep convective mixing towards the onset of the summer monsoon and weak horizontal winds (Ojha et al., 2014; Naja et al., 2016) leading to the accumulation of the photochemically processed air masses of tropospheric origin.

Since the LRT over this region is located significantly higher (Fig. 4, also see Naja et al., 2016) than the altitude of SOPs, and that the ozone in SOPs is found to be of stratospheric origin, we conclude that stratospheric air masses are sandwiched between tropospheric layers at 10–11 km altitude. This result complements previous studies, primarily showing the altitudinal placement of SOPs at about 14 km

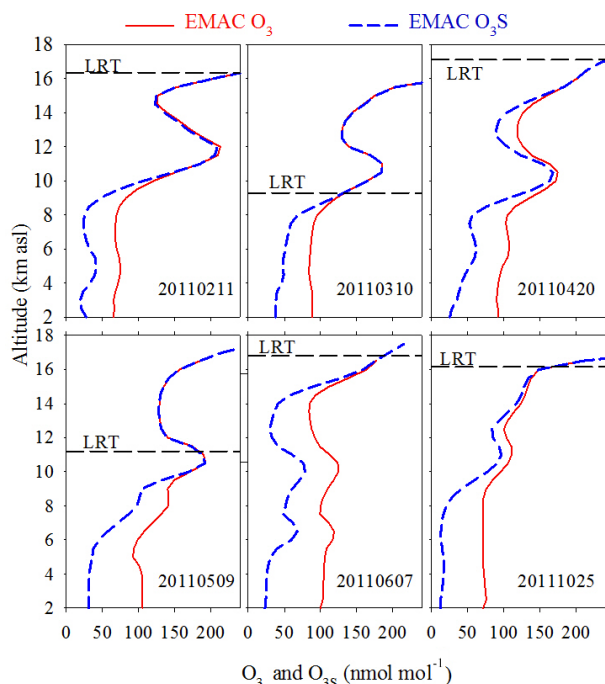


Figure 4. Vertical profiles of EMAC-simulated ozone and stratospheric ozone tracer (O_{3s}) during the SOPs over Nainital. The height of the lapse rate tropopause (LRT) from EMAC, calculated using the WMO definition, is also shown.

near the lower stratosphere (UTLS) (e.g. Reid and Vaughan, 1991; Hwang et al., 2007).

In order to investigate the underlying dynamics that transport the stratospheric air masses, leading to SOPs over the Himalayas, we analysed the backward air trajectories (Supplement, Fig. S4) initialized over Nainital at 10, 11 and 12 km, which are the typical altitudes of the SOPs (Fig. 2). The air mass trajectories indicate rapid transport from the west; for example on 11 February, it took only 2 days for the air masses to be transported across Africa and the Middle East and reach the Himalayas. Further, the locations of the tropopause folds occurred during the period of air trajectories are also shown. The tropopause folds are mostly found in a belt between about 20 and 35° N, in agreement with previous studies (Škerlak et al., 2015). The air masses encountered extensive tropopause dynamics along the path of transport before reaching the Himalayas.

Additionally, air mass trajectories were computed for each model time step during May 2002 in which the frequency of SOPs was found to be the highest during the 2000–2014 period. Figures 6 shows the EMAC-simulated evolution of O_{3s} along these trajectories classified into SOPs and non-SOPs above Nainital. The evolution of O_3 and PV along the trajectories are shown in the Supplement (Figs. S7 and S8). Air masses are enriched/accumulate the ozone of stratospheric origin during transport to Nainital, causing SOPs. A significant fraction of trajectories during non-SOP time steps origi-

nates over the south-west with lower O_{3s} ($< 90 \text{ nmol mol}^{-1}$). The trajectories which do get higher contributions of stratospheric ozone are found to be diluted during transport, making the enhancements above Nainital too small to be an SOP.

The vertical distribution of EMAC-simulated O_{3s}/O_3 ratio along the 5-day backward air trajectories are shown in Fig. 7. The pressure variations of the air masses and tropopause along the trajectory are also shown. The O_{3s}/O_3 ratio is mostly found to be close to unity (≥ 0.9) near the altitude (pressure) of air mass trajectory during transport, except on 7 June and 25 October (0.5–0.8). The intrusions enriching tropospheric air masses with stratospheric O_3 are clearly visible. More specifically, a significant stratospheric contribution to tropospheric ozone is found in the upper–middle troposphere during the 5-day period before the event, with the associated PV values ($< 2 \text{ pvu}$), indicating mixing of stratospheric air into the troposphere. Additionally, strong variability in the altitude of the LRT along the path of the transport is seen, except for the event of 7 June. The dramatic variability in the LRT along the trajectory (e.g. from 100 to 200 hPa on 11 February) appears to be associated with the tropopause-folding activity (Figs. S4 and S5). Several shallow tropopause folds (vertical extent of 50 to 200 hPa) occur along the transport path, while medium folds (vertical extent of 200–350 hPa) are only found during 11 February and 9 May. Intrusion of a significant amount of O_3 due to tropopause folds over the eastern Mediterranean and the Middle East was shown by Akritidis et al. (2016). The combination of very strong winds associated with the subtropical jets (Fig. S4, Ojha et al., 2014; Naja et al., 2016) and this intense tropopause dynamics, enriching the troposphere with stratospheric ozone, leads to the formation of SOPs over the Himalayas.

The transport of ozone-rich air masses from the stratosphere towards the Himalayas can be seen more clearly in the longitude–pressure cross sections at 30° N (Fig. 8), and latitude–pressure cross sections at 80° E (Fig. 9) for all the events and the day before. Figure 8 reveals three geographical regions viz. northern Africa and Atlantic Ocean ($\text{lon} < 40^\circ \text{ E}$), the Middle East ($40\text{--}60^\circ \text{ E}$) and northern South Asia ($60\text{--}100^\circ \text{ E}$), where the intrusions of stratospheric air masses can be identified. Blobs of air masses characterized by high PV values ($> 2 \text{ PVU}$) are also seen. Additionally, Fig. 9 shows that stratospheric influences are more pronounced over the northern parts of the Indian subcontinent compared to southern India. This result based on EMAC simulations is found to be in agreement with the study by Ganguly and Tzani (2011) based on ozone-sonde observations at three Indian stations.

To investigate the possible mixing of the transported stratospheric air with tropospheric air in the vicinity of the SOPs, the turbulence index (TI) is derived from EMAC fields, as described in Ellrod and Knapp (1992). To detect the clear air turbulence (CAT) areas and potential mixing, an approach similar to that of Traub and Lelieveld (2003)

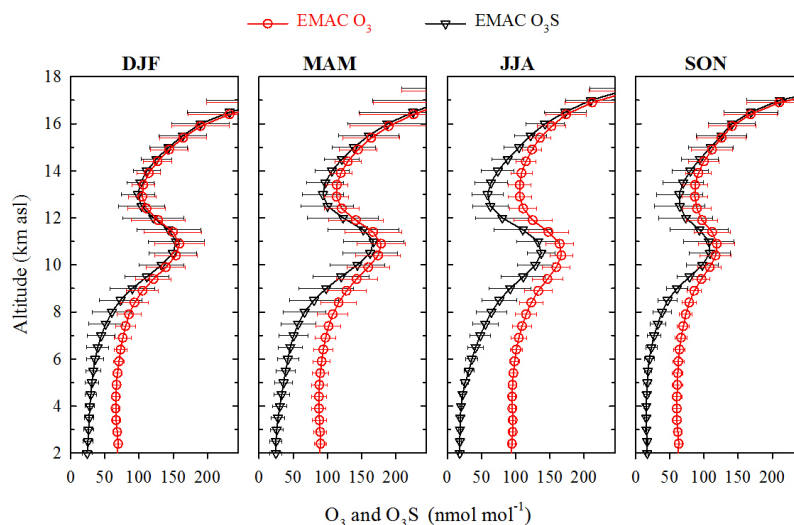


Figure 5. Average vertical profiles of EMAC-simulated ozone (O_3) and stratospheric ozone tracer (O_3S) during the SOPs over Nainital aggregated into four seasons: DJF (winter), MAM (spring/pre-monsoon), JJA (summer monsoon), and SON (autumn) for the period 2000–2014.

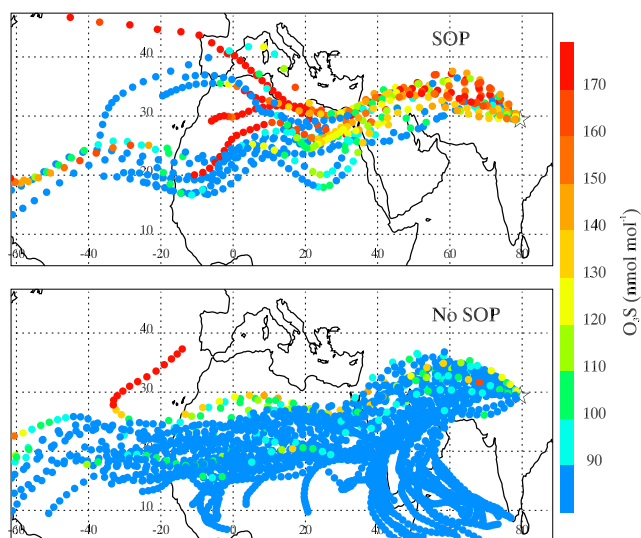


Figure 6. EMAC-simulated evolution of O_3s along 5-day backward air trajectories over Nainital during SOPs and non-SOPs with starting altitude of 11 km for the month May 2002. The difference between symbols on trajectories represent a time period of 3 h. The location of the Nainital site is shown by the star symbol.

has been followed. The pressure-longitude cross sections of O_3s (colour filled) and TI (contour lines) at 29.5°N near the SOPs pressure height (400–100 hPa) are shown in the Fig. 10 for the time steps of events and a time step before and after the event. The enhanced TI values during the SOP events above Nainital indicate higher probability of mixing between stratospheric and tropospheric air, supporting the irreversible nature of the associated STT.

3.3 Frequency of SOPs

The frequency of SOP occurrences was not estimated over Nainital from the observations, due to the availability of only 3–4 profiles in each month. However a tendency of higher frequency during spring was noticed (three events) compared to other seasons (one event per season) (Ojha et al., 2014). In this section, we use long-term EMAC simulations, conducted for a period of 15 years (2000–2014), to investigate the frequency of SOP occurrence and seasonality over the central Himalayas. Due to the variability in the SOP altitude as well as the absolute enhancements during the SOPs, general/unique criteria cannot be defined. Therefore, we first select the ozone profiles in which average ozone mixing ratios (AOMR) at 10–12 km, a typical altitude of SOP occurrence, are significantly higher (at least by 50 %) compared to average ozone in the lower troposphere. Additionally, to explicitly select only the profiles which are SOPs (and not a direct intrusion over the Himalayas) a criterion was applied that directly above the SOP the ozone mixing ratios should again be lower (at least by 20 %) so that selected profiles have a shape typical of SOPs, as shown in Fig. 2. These two conditions can be mathematically expressed as

$$\text{AOMR}^{10-12\text{km}} \geq 1.5 \times \text{AOMR}^{0-6\text{km}},$$

and

$$\text{AOMR}^{12-14\text{km}} \leq 0.8 \times \text{AOMR}^{10-12\text{km}}.$$

Further, the factors 1.5 and 0.8, representing an enhancement by 50 % and reduction by 20 %, were suitably varied, which confirmed the generality of the result (not shown). We calculated the frequencies of occurrence in percentage

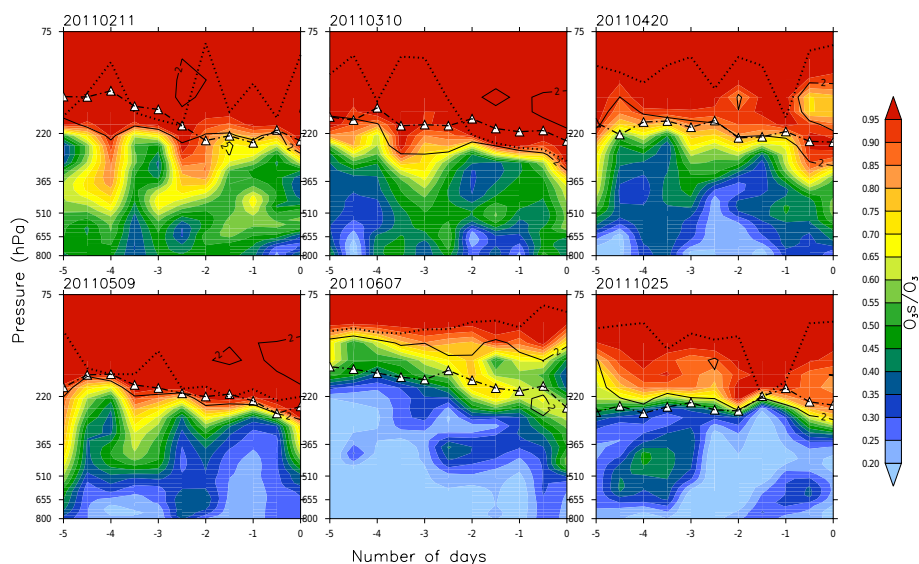


Figure 7. The vertical distribution of EMAC-simulated O_3s/O_3 ratio along the trajectories with starting altitude of 11 km over Nainital. The x axis shows the number of days backward in time and the y axis shows the pressure in hPa. White filled triangles show the pressure along the back-trajectory and the difference between two consecutive symbols on the line represent a time period of 12 h. The dotted black line indicates the tropopause (LRT). The solid black line is the 2 PVU contour.

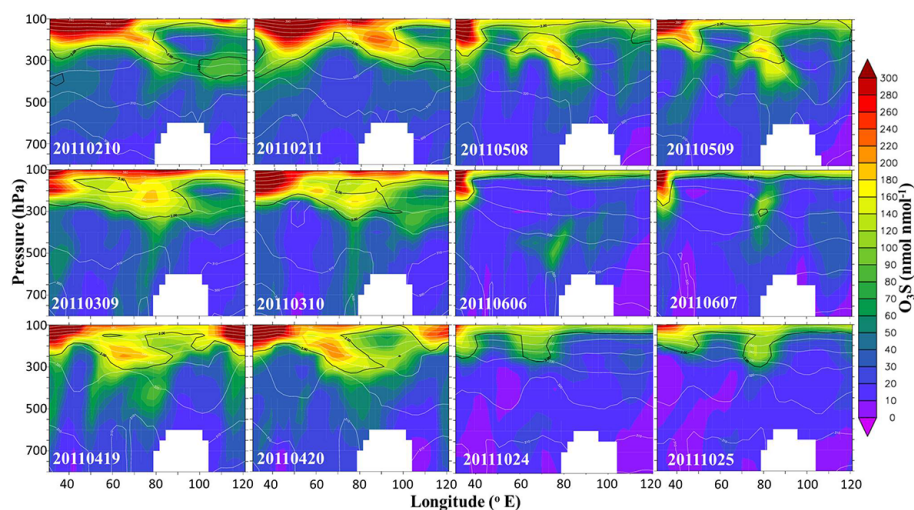


Figure 8. The longitude-pressure cross section of EMAC-simulated O_3s at 29.5° N during all SOP days and a day before the event. White lines denote the potential temperature (K) and the black line denotes the dynamical tropopause at 2 PVU.

for each month during 2000–2014, and converted these to an average climatological seasonal cycle (Fig. 11). Standard deviations in a month represent the variability in the SOP frequency in different years during the 2000–2014 period.

The highest frequency of SOPs over the central Himalayas is found during the pre-monsoon season (MAM), followed by winter (DJF). The frequency of SOP occurrences over Nainital increases steadily from January (2.7 %) to May (10.8 %), and abruptly declines in June (1.2 %). The model does not predict any SOPs during July–October. It should be noted that here we included only events which show en-

hancements by at least 50 % as SOPs; therefore some events with smaller enhancements could be present during July–October. It is suggested that the more frequent stratospheric intrusions during spring combined with the stronger horizontal advection lead to more frequent SOP events. Seasonal composites of the spatial locations of folds (Fig. S6) show a higher frequency of occurrence during SOPs. The effects of stronger cross-tropopause exchange and influx of the stratospheric air masses during spring and winter over the Himalayas and surrounding regions, such as in southern parts of the Tibetan Plateau, have also been shown by Škerlak et al.

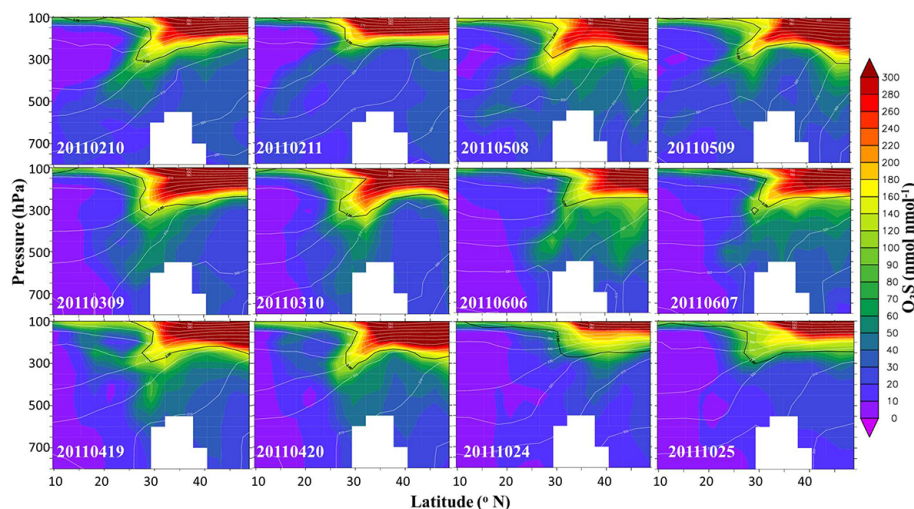


Figure 9. The latitude–pressure cross section of EMAC-simulated O_3 s at 79.5° E during all SOP days and a day before the event. White lines denote the potential temperature (K) and the black line denotes the dynamical tropopause at 2 PVU.

(2014, 2015). The frequency of SOP events over this region is minimum during the summer monsoon season, as the weak horizontal winds (Ojha et al., 2014; Naja et al., 2016) do not transport the ozone from STTs over large distances. The frequency of stratospheric intrusions and tropopause folds over the Himalayas and surrounding regions are lower during the summer monsoon (Cristofanelli et al., 2010; Putero et al., 2016). Multiple tropopauses that can occur in winter and spring over the Tibetan Plateau are shown to be absent during the summer monsoon season (Chen et al., 2011). Additionally, stronger vertical mixing due to monsoonal convection prevents high ozone layers from forming and being sustained. These findings are in agreement with the ground-based ozone measurements in the southern Himalayas, where about 78 % of the stratospheric influences were attributed to the PV structures induced by fluctuations of the zonal flow and tropopause fold development along the subtropical jet stream, while monsoon depressions only account for 3 % of the events (Bracci et al., 2012). Further, the seasonality of SOP frequency derived from EMAC simulations is consistent with the conclusions based on the limited number of observational profiles in Ojha et al. (2014). Next we determine the enhancements in tropospheric ozone columns due to the presence of SOPs over the central Himalayas.

3.4 Effect of SOPs on tropospheric column ozone

Figure 12 shows the climatological mean seasonal cycle of the tropospheric column ozone (TCO) in Dobson units (DU) over Nainital from EMAC simulations over the period 2000–2014. TCO values are calculated by integrating ozone mixing ratios up to the LRT, determined using the WMO definition. To investigate the effect of SOPs on TCO, we compare three TCO values: first using EMAC-simulated O_3 values from all time steps, second by selecting only the time steps when

there is an SOP event as per the criteria discussed in Sect. 3.3, and third by taking all time steps when SOPs do not occur.

TCO values for the all-time and non-SOP conditions are found to be very similar, mainly due to the large number of data counts (more than 1000 data counts in individual month) compared to those in SOPs (0–120 data counts in an individual month). The maxima of TCO during May and June (54.7 ± 5.9 and 55.0 ± 4.4 DU respectively) are attributed to the intense solar radiation and high pollution loading over northern India. Photochemical production of ozone is less efficient during the winter (TCO: 33.7 ± 3.6 to 37.6 ± 5.8 DU) and the summer monsoon (e.g. 44.9 ± 4.9 DU in August). Overall, the EMAC-simulated TCO seasonality from all data is found to be consistent with satellite data (Ojha et al., 2012) over this region.

The occurrences of SOPs are seen to clearly enhance the TCO values in winter, pre-monsoon and early summer. To estimate the enhancement in the tropospheric ozone that would likely persist in the troposphere (not reversible), an additional criterion of PV values up to 2 PVU has been applied here.

The maximum enhancement in climatological average TCO value due to SOPs is found during January, when TCO values during SOPs (43.5 ± 3.0 DU) are higher by as much as 7.5 DU (21 %) compared to the non-SOP time steps (36.0 ± 3.6 DU). The enhancements in tropospheric ozone loading over the central Himalayas due to SOPs are estimated to be 3.3–7.5 DU (6–21 %) from January to June. Additional calculations, which relax the PV criteria to include SOP time steps having PV values higher than 2 PVU as well, lead to slightly higher values of the estimated enhancement (4–9 DU: 7–26 %) on the TCO.

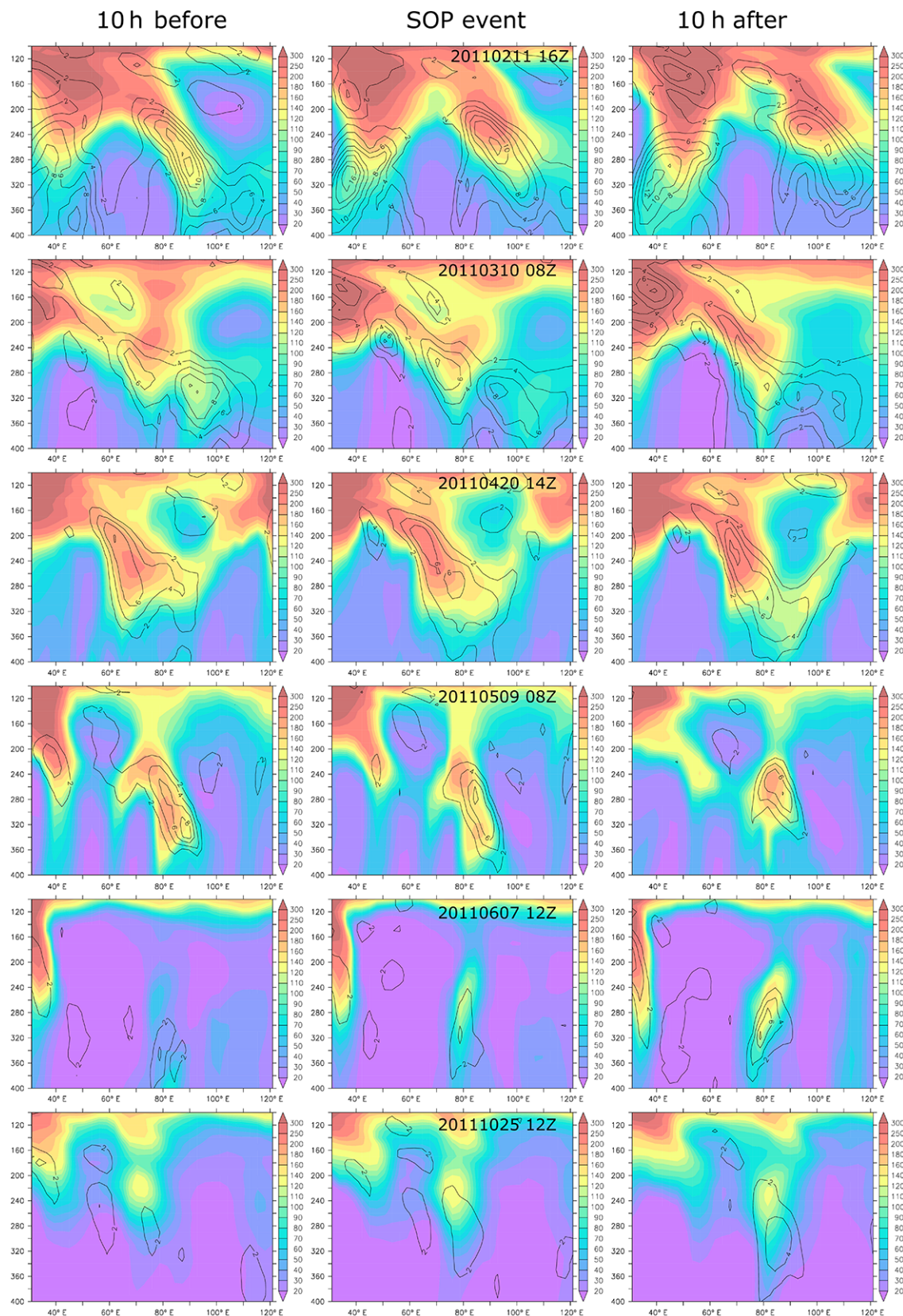


Figure 10. The longitude–pressure cross section of O_3s (colour filled), and turbulence index (TI) (contour lines) (in $10^{-7} s^{-2}$) at $29.5^\circ N$.

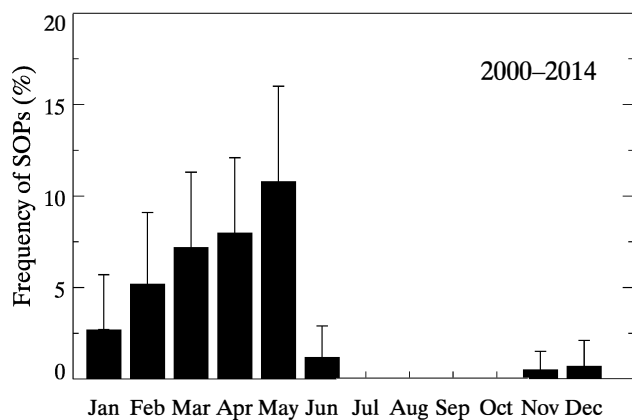


Figure 11. Annual cycle of SOP occurrence frequency (%) over Nainital, calculated from the EMAC simulations for the period 2000–2014. The error bars show the standard deviation of SOP frequency during each month among different years 2000–2014 period.

4 Conclusions

In this study, we used the EMAC model to investigate the layers of high ozone mixing ratios (SOPs) in the middle–upper troposphere, observed over the central Himalayas in northern India. EMAC successfully reproduces the occurrence, altitudinal placement and the relative ozone enhancements during SOP events observed in ozone-sonde profiles. The vertical profiles calculated by long-term EMAC simulations show layers of high PV (1.8 ± 0.5 – 3.0 ± 1.3 PVU) coinciding with the altitude of SOPs, which suggests influences from stratospheric intrusions. The analysis of O_3s further shows that generally all excess ozone at SOP altitudes over the Himalayas is transported from the stratosphere. Average O_3s at the SOP altitudes is estimated to be maximum during the spring (162.5 ± 40 nmol mol⁻¹), followed by winter (149.4 ± 35 nmol mol⁻¹). Tropospheric photochemical sources are found to contribute significantly to the SOPs and above during the summer monsoon (30 nmol mol⁻¹).

Analysis of backward air trajectories in conjunction with EMAC-simulated O_3 distributions and tropopause dynamics revealed that stratospheric air masses are sandwiched between tropospheric layers at 10–11 km altitude due to tropopause folds which are rapidly transported along the subtropical jet to cause SOP structures over the Himalayas. In contrast to SOP time steps, a fraction of air mass trajectories during non SOP time steps are from the south west, which have significantly lower contributions of stratospheric ozone. Regions as far as northern Africa and the Atlantic Ocean, the Middle East and northern South Asia are found to be regions of stratospheric intrusions that act as sources of high ozone mixing ratios. The distribution of O_3s showed that STT effects are more pronounced over the northern Indian subcontinent than those over southern India.

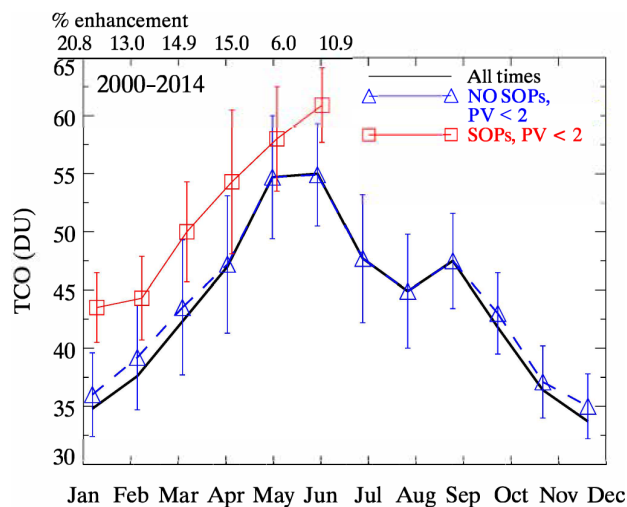


Figure 12. Annual cycle of EMAC-simulated TCO over the central Himalayas calculated from (1) all EMAC time steps (all times), (2) only the time steps having SOPs (SOPs), and (3) only when SOPs are not present (non-SOPs) over the period 2000–2014. Enhancements in TCO values (in %) during SOPs compared to non-SOPs are also indicated. TCO values for SOPs and non-SOPs are derived only when the average PV value at 10–12 km is up to 2 PVU. Error bars represent the standard deviation derived from the temporal variations over the period of 2000–2014.

We used long-term model simulations (2000–2014) to calculate the frequency of SOP occurrence showing maxima during spring (about 11 % of the time in May), while no SOPs were predicted during the July–October months. This is consistent with results based on ozone soundings over the region. The high frequency of SOPs during spring is attributed to the occurrence of stratospheric intrusions combined with rapid horizontal transport. The minima in the frequency of SOPs during the summer monsoon are partially due to much weaker horizontal transport due to the northward displacement of subtropical jet stream and stronger monsoonal convective mixing. Model simulations were further used to investigate the effect of SOPs on the TCO. The EMAC-simulated TCO seasonality is in agreement with satellite data. SOP occurrence is found to significantly enhance the TCO over the region by 3.3–7.5 DU (6–21 %). Such an enhancement in tropospheric ozone at the SOP altitude could translate to an increase in surface temperature by 0.06 to 0.13 °C, based on the vertical profile of ozone forcing (Lacis et al., 1990). Additionally, as expected due to their origin from dynamical processes, the occurrences of SOPs discern very large interannual variability (see e.g. Supplement, Fig. S9), which highlights a need for in situ measurements and numerical simulations on climatic timescales to quantify the role of SOPs in measured ozone trends over Asian regions, especially in the middle–upper troposphere (Banerjee et al., 2016; Tanimoto et al., 2016) and their impacts on tropospheric chemistry and climate.

Data availability. The EMAC simulations conducted as part of the ESCiMo project will be made available in the Climate and Environmental Retrieval and Archive (CERA) database at the German Climate Computing Centre (DKRZ; <http://cera-www.dkrz.de/WDCC/ui/Index.jsp>). The corresponding digital object identifiers (DOI) will be published on the MESSy consortium web-page (<http://www.messy-interface.org>). A subset of the data of those simulations consistently covering the requested time periods (1960–2010 for RC1, and 1960–2009 for RC2) will be submitted to the BADC database for the CCMi project. Ozone profiles for Nainital used in the paper and Delhi used in the Supplement are obtained from a previous study (Ojha et al., 2014) and WOUDC database (<http://woudc.org/data/explore.php>) respectively.

The Supplement related to this article is available online at <https://doi.org/10.5194/acp-17-6743-2017-supplement>.

Competing interests. The authors declare that they have no conflict of interest.

Acknowledgements. The model simulations have been performed at the German Climate Computing Centre (DKRZ) through support from the Bundesministerium für Bildung und Forschung (BMBF). DKRZ and its scientific steering committee are gratefully acknowledged for providing the HPC and data archiving resources for this consortial project ESCiMo (Earth System Chemistry integrated Modelling). The authors gratefully acknowledge the NOAA Air Resources Laboratory (ARL) for the provision of the HYSPLIT transport and dispersion model and READY website (<http://www.ready.noaa.gov>) used in this publication. Constructive comments and suggestions from the two anonymous reviewers are gratefully acknowledged.

The article processing charges for this open-access publication were covered by the Max Planck Society.

Edited by: F. Fierli

Reviewed by: two anonymous referees

References

- Akritidis, D., Pozzer, A., Zanis, P., Tyrlis, E., Škerlak, B., Sprenger, M., and Lelieveld, J.: On the role of tropopause folds in summertime tropospheric ozone over the eastern Mediterranean and the Middle East, *Atmos. Chem. Phys.*, 16, 14025–14039, <https://doi.org/10.5194/acp-16-14025-2016>, 2016.
- Banerjee, A., Maycock, A. C., Archibald, A. T., Abraham, N. L., Telford, P., Braesicke, P., and Pyle, J. A.: Drivers of changes in stratospheric and tropospheric ozone between year 2000 and 2100, *Atmos. Chem. Phys.*, 16, 2727–2746, <https://doi.org/10.5194/acp-16-2727-2016>, 2016.

- Bracci, A., Cristofanelli, P., Sprenger, M., Bonafè, U., Calzolari, F., Duchi, R., Laj, P., Marinoni, A., Roccatto, F., Vuillermoz, E., and Bonasoni, P.: Transport of Stratospheric Air Masses to the Nepal Climate Observatory–Pyramid (Himalaya; 5079 m MSL): A Synoptic-Scale Investigation, *J. Appl. Meteorol. Clim.*, 51, 1489–1507, <https://doi.org/10.1175/JAMC-D-11-0154.1>, 2012.
- Chen, X. L., Ma, Y. M., Kelder, H., Su, Z., and Yang, K.: On the behaviour of the tropopause folding events over the Tibetan Plateau, *Atmos. Chem. Phys.*, 11, 5113–5122, <https://doi.org/10.5194/acp-11-5113-2011>, 2011.
- Cristofanelli, P., Bracci, A., Sprenger, M., Marinoni, A., Bonafè, U., Calzolari, F., Duchi, R., Laj, P., Pichon, J. M., Roccatto, F., Venzac, H., Vuillermoz, E., and Bonasoni, P.: Tropospheric ozone variations at the Nepal Climate Observatory–Pyramid (Himalayas, 5079 m a.s.l.) and influence of deep stratospheric intrusion events, *Atmos. Chem. Phys.*, 10, 6537–6549, <https://doi.org/10.5194/acp-10-6537-2010>, 2010.
- Das, S. S., Ratnam, M. V., Uma, K. N., Subrahmanyam, K. V., Girach, I. A., Patra, A. K., Aneesh, S., Suneeth, K. V., Kumar, K. K., Kesarkar, A. P., Sijikumar, S., and Ramkumar, G.: Influence of tropical cyclones on tropospheric ozone: possible implications, *Atmos. Chem. Phys.*, 16, 4837–4847, <https://doi.org/10.5194/acp-16-4837-2016>, 2016.
- Dee, D. P., Uppala, S. M., Simmons, A. J., Berrisford, P., Poli, P., Kobayashi, S., Andrae, U., Balmaseda, M. A., Balsamo, G., Bauer, P., Bechtold, P., Beljaars, A. C. M., van de Berg, L., Bidlot, J., Bormann, N., Delsol, C., Dragani, R., Fuentes, M., Geer, A. J., Haimberger, L., Healy, S. B., Hersbach, H., Hølm, E. V., Isaksen, I., Kållberg, P., Köhler, M., Matricardi, M., McNally, A. P., Monge-Sanz, B. M., Morcrette, J.-J., Park, B.-K., Peubey, C., de Rosnay, P., Tavolato, C., Thépaut, J.-N., and Vitart, F.: The ERA-Interim reanalysis: configuration and performance of the data assimilation system, *Q. J. Roy. Meteor. Soc.*, 137, 553–597, <https://doi.org/10.1002/qj.828>, 2011.
- Dobson, G.: The laminated structure of the ozone in the atmosphere, *Q. J. Roy. Meteor. Soc.*, 99, 599–607, 1973.
- Draxler, R. and Hess, G.: Description of the HYSPLIT 4 modeling system, NOAA Tech. Memo. ERL ARL-224, NOAA Air Resources Laboratory, Silver Spring, MD, 24 pp., 1997.
- Draxler, R. and Hess, G.: An overview of the HYSPLIT 4 modeling system of trajectories, dispersion, and deposition, *Aust. Meteorol. Mag.*, 47, 295–308, 1998.
- Draxler, R., Stunder, B., Rolph, G., Stein, A., and Taylor, A.: HYSPLIT4 USER'S GUIDE, available at: http://www.arl.noaa.gov/documents/reports/hysplit_user_guide.pdf (last access: 6 June 2017), 2014.
- Ellrod, G. and Knapp, D.: An Objective Clear-Air Turbulence Forecasting Technique: Verification and Operational Use, *Weather Forecast.*, 7, 150–165, [https://doi.org/10.1175/1520-0434\(1992\)007<0150:AOCATF>2.0.CO;2](https://doi.org/10.1175/1520-0434(1992)007<0150:AOCATF>2.0.CO;2), 1992.
- Fadnavis, S., Chakraborty, T., and Beig, G.: Seasonal stratospheric intrusion of ozone in the upper troposphere over India, *Ann. Geophys.*, 28, 2149–2159, <https://doi.org/10.5194/angeo-28-2149-2010>, 2010.

- Fishman, J., Wozniak, A. E., and Creilson, J. K.: Global distribution of tropospheric ozone from satellite measurements using the empirically corrected tropospheric ozone residual technique: Identification of the regional aspects of air pollution, *Atmos. Chem. Phys.*, 3, 893–907, <https://doi.org/10.5194/acp-3-893-2003>, 2003.
- Ganguly, N. D. and Tzani, C.: Study of Stratosphere-troposphere exchange events of ozone in India and Greece using ozonesonde ascents, *Meteorol. Appl.*, 18, 467–474, <https://doi.org/10.1002/met.241>, 2011.
- Holton, J. R. and Lelieveld, J.: Stratosphere-Troposphere Exchange and its role in the budget of tropospheric ozone, 173–190, Springer Berlin Heidelberg, Berlin, Heidelberg, https://doi.org/10.1007/978-3-642-61051-6_8, 1996.
- Hwang, S.-H., Kim, J., Won, Y.-I., Cho, H. K., Kim, J. S., Lee, D.-H., Cho, G.-R., and Oh, S. N.: Statistical characteristics of secondary ozone density peak observed in Korea, *Adv. Space Res.*, 36, 952–957, <https://doi.org/10.1016/j.asr.2005.05.080>, 2005.
- Hwang, S.-H., Kim, J., and Cho, G.-R.: Observation of secondary ozone peaks near the tropopause over the Korean peninsula associated with stratosphere-troposphere exchange, *J. Geophys. Res.-Atmos.*, 112, d16305, <https://doi.org/10.1029/2006JD007978>, 2007.
- Jöckel, P., Kerkweg, A., Pozzer, A., Sander, R., Tost, H., Riede, H., Baumgaertner, A., Gromov, S., and Kern, B.: Development cycle 2 of the Modular Earth Submodel System (MESSy2), *Geosci. Model Dev.*, 3, 717–752, <https://doi.org/10.5194/gmd-3-717-2010>, 2010.
- Jöckel, P., Tost, H., Pozzer, A., Kunze, M., Kirner, O., Brenninkmeijer, C. A. M., Brinkop, S., Cai, D. S., Dyroff, C., Eckstein, J., Frank, F., Garny, H., Gottschaldt, K.-D., Graf, P., Grewe, V., Kerkweg, A., Kern, B., Matthes, S., Mertens, M., Meul, S., Neumaier, M., Nützel, M., Oberländer-Hayn, S., Ruhnke, R., Runde, T., Sander, R., Scharffe, D., and Zahn, A.: Earth System Chemistry integrated Modelling (ESCI-Mo) with the Modular Earth Submodel System (MESSy) version 2.51, *Geosci. Model Dev.*, 9, 1153–1200, <https://doi.org/10.5194/gmd-9-1153-2016>, 2016.
- Kumar, A., Ram, K., and Ojha, N.: Variations in carbonaceous species at a high-altitude site in western India: Role of synoptic scale transport, *Atmos. Environ.*, 125, 371–382, <https://doi.org/10.1016/j.atmosenv.2015.07.039>, 2015.
- Lacis, A. A., Wuebbles, D. J., and Logan, J. A.: Radiative forcing of climate by changes in the vertical distribution of ozone, *J. Geophys. Res.-Atmos.*, 95, 9971–9981, <https://doi.org/10.1029/JD095iD07p09971>, 1990.
- Lal, S., Venkataramani, S., Srivastava, S., Gupta, S., Mallik, C., Naja, M., Sarangi, T., Acharya, Y. B., and Liu, X.: Transport effects on the vertical distribution of tropospheric ozone over the tropical marine regions surrounding India, *J. Geophys. Res.-Atmos.*, 118, 1513–1524, <https://doi.org/10.1002/jgrd.50180>, 2013.
- Lelieveld, J. and Dentener, F. J.: What controls tropospheric ozone?, *J. Geophys. Res.-Atmos.*, 105, 3531–3551, <https://doi.org/10.1029/1999JD901011>, 2000.
- Lemoine, R.: Secondary maxima in ozone profiles, *Atmos. Chem. Phys.*, 4, 1085–1096, <https://doi.org/10.5194/acp-4-1085-2004>, 2004.
- Logan, J. A.: Tropospheric ozone: Seasonal behavior, trends and anthropogenic influence, *J. Geophys. Res.*, 90, 10463–10482, 1985.
- Logan, J. A.: Trends in the vertical distribution of ozone: an analysis of ozonesonde data, *J. Geophys. Res.*, 99, 25553–25585, 1994.
- Mandal, T. K., Cho, J. Y. N., Rao, P. B., Jain, A. R., Peshin, S. K., Srivastava, S. K., Bohra, A. K., and Mitra, A. P.: Stratosphere-troposphere ozone exchange observed with the Indian MST radar and a simultaneous balloon-borne ozonesonde, *Radio Sci.*, 33, 861–893, <https://doi.org/10.1029/97RS03553>, 1998.
- Monks, P. S., Archibald, A. T., Colette, A., Cooper, O., Coyle, M., Derwent, R., Fowler, D., Granier, C., Law, K. S., Mills, G. E., Stevenson, D. S., Tarasova, O., Thouret, V., von Schneidemesser, E., Sommariva, R., Wild, O., and Williams, M. L.: Tropospheric ozone and its precursors from the urban to the global scale from air quality to short-lived climate forcer, *Atmos. Chem. Phys.*, 15, 8889–8973, <https://doi.org/10.5194/acp-15-8889-2015>, 2015.
- Myhre, G., Shindell, D., Breon, F.-M., Collins, W., Fuglestedt, J., Huang, J., Koch, D., Lamarque, J.-F., Lee, D., Mendoza, B., Nakajima, T., Robock, A., Stephens, G., Takemura, T., and Zhang, H.: Anthropogenic and Natural Radiative Forcing, in: *Climate Change 2013: The Physical Science Basis. Contribution of Working Group I to the Fifth Assessment Report of the Intergovernmental Panel on Climate Change*, edited by: Stocker, T. F., Qin, D., Plattner, G.-K., Tignor, M., Allen, S. K., Boschung, J., Nauels, A., Xia, Y., Bex, V., and Midgley, P. M., Cambridge University Press, 2013.
- Naja, M., Bhardwaj, P., Singh, N., Kumar, P., Kumar, R., Ojha, N., Sagar, R., Satheesh, S. K., Krishna Moorthy, K., and Kotamarthi, V. R.: High-frequency vertical profiling of meteorological parameters using AMF1 facility during RAWEX-GVAX at ARIES, Nainital, *Curr. Sci.*, 110, 2317–2325, <https://doi.org/10.18520/cs/v111/i1/132-140>, 2016.
- Neu, J. L., Flury, T., Manney, G. L., Santee, M. L., Livesey, N. J., and Worden, J.: Tropospheric ozone variations governed by changes in stratospheric circulation, *Nat. Geosci.*, 7, 340–344, <https://doi.org/10.1038/NGEO2138>, 2014.
- Ojha, N., Naja, M., Singh, K. P., Sarangi, T., Kumar, R., Lal, S., Lawrence, M. G., Butler, T. M., and Chandola, H. C.: Variabilities in ozone at a semi-urban site in the Indo-Gangetic Plain region: Association with the meteorology and regional processes, *J. Geophys. Res.-Atmos.*, 117, D20301, <https://doi.org/10.1029/2012JD017716>, 2012.
- Ojha, N., Naja, M., Sarangi, T., Kumar, R., Bhardwaj, P., Lal, S., Venkataramani, S., Sagar, R., Kumar, A., and Chandola, H.: On the processes influencing the vertical distribution of ozone over the central Himalayas: Analysis of year-long ozonesonde observations, *Atmos. Environ.*, 88, 201–211, <https://doi.org/10.1016/j.atmosenv.2014.01.031>, 2014.
- Ojha, N., Pozzer, A., Rauthe-Schöch, A., Baker, A. K., Yoon, J., Brenninkmeijer, C. A. M., and Lelieveld, J.: Ozone and carbon monoxide over India during the summer monsoon: regional emissions and transport, *Atmos. Chem. Phys.*, 16, 3013–3032, <https://doi.org/10.5194/acp-16-3013-2016>, 2016.

- Park, S. S., Kim, J., Cho, H. K., Lee, H., Lee, Y., and Miyagawa, K.: Sudden increase in the total ozone density due to secondary ozone peaks and its effect on total ozone trends over Korea, *Atmos. Environ.*, 47, 226–235, <https://doi.org/10.1016/j.atmosenv.2011.11.011>, 2012.
- Pozzer, A., Jöckel, P., Tost, H., Sander, R., Ganzeveld, L., Kerkweg, A., and Lelieveld, J.: Simulating organic species with the global atmospheric chemistry general circulation model ECHAM5/MESSEy1: a comparison of model results with observations, *Atmos. Chem. Phys.*, 7, 2527–2550, <https://doi.org/10.5194/acp-7-2527-2007>, 2007.
- Pozzer, A., Pollmann, J., Taraborrelli, D., Jöckel, P., Helmig, D., Tans, P., Hueber, J., and Lelieveld, J.: Observed and simulated global distribution and budget of atmospheric C₂–C₅ alkanes, *Atmos. Chem. Phys.*, 10, 4403–4422, <https://doi.org/10.5194/acp-10-4403-2010>, 2010.
- Pozzer, A., de Meij, A., Pringle, K. J., Tost, H., Doering, U. M., van Aardenne, J., and Lelieveld, J.: Distributions and regional budgets of aerosols and their precursors simulated with the EMAC chemistry-climate model, *Atmos. Chem. Phys.*, 12, 961–987, <https://doi.org/10.5194/acp-12-961-2012>, 2012.
- Putero, D., Cristofanelli, P., Sprenger, M., Škerlak, B., Tositti, L., and Bonasoni, P.: STEFLUX, a tool for investigating stratospheric intrusions: application to two WMO/GAW global stations, *Atmos. Chem. Phys.*, 16, 14203–14217, <https://doi.org/10.5194/acp-16-14203-2016>, 2016.
- Ramanathan, V., Ramana, M. V., Roberts, G., Kim, D., Corrigan, C., Chung, C., and Winker, D.: Warming trends in Asia amplified by brown cloud solar absorption, *Nature*, 448, 575–578, <https://doi.org/10.1038/nature06019>, 2007.
- Ramanathan, V., Agrawal, M., Akimoto, H., Aufhammer, M., Devotta, S., Emberson, L., Hasnain, S. I., Iyengararasan, M., Jayaraman, A., Lawrance, M., Nakajima, T., Oki, T., Rodhe, H., Ruchirawat, M., Tan, S. K., Vincent, J., Y., W. J., Yang, D., Zhang, Y. H., Autrup, H., Barregard, L., Bonasoni, P., Brauer, M., Brunekreef, B., Carmichael, G., Chung, C. E., Dahe, J., Feng, Y., Fuzzi, S., Gordon, T., Gosain, A. K., Htun, N., Kim, J., Mourato, S., Naeher, L., Navasumrit, P., Ostro, B., Panwar, T., Rahman, M. R., Ramana, M. V., Rupakheti, M., Settachan, D., Singh, A. K., Helen, G. S., Tan, P. V., Viet, P. H., Yinlong, J., Yoon, S. C., Chang, W.-C., Wang, X., Zelikoff, J., and Zhu, A.: Atmospheric Brown Clouds: Regional Assessment Report with Focus on Asia, United Nations Environment Programme, Nairobi, Kenya, 2008.
- Reid, S. J. and Vaughan, G.: Lamination in ozone profiles in the lower stratosphere, *Q. J. Roy. Meteor. Soc.*, 117, 825–844, 1991.
- Roeckner, E., Brokopf, R., Esch, M., Giorgetta, M., Hagemann, S., Kornblüeh, L., Manzini, E., Schlese, U., and Schulzweida, U.: Sensitivity of Simulated Climate to Horizontal and Vertical Resolution in the ECHAM5 Atmosphere Model, *J. Climate*, 19, 3771–3791, <https://doi.org/10.1175/JCLI3824.1>, 2006.
- Roelofs, G.-J. and Lelieveld, J.: Model study of the influence of cross-tropopause O₃ transports on tropospheric O₃ levels, *Tellus B*, 49, 38–55, <https://doi.org/10.1034/j.1600-0889.49.issue1.3.x>, 1997.
- Sarangi, T., Naja, M., Ojha, N., Kumar, R., Lal, S., Venkataramani, S., Kumar, A., Sagar, R., and Chandola, H. C.: First simultaneous measurements of ozone, CO, and NO_y at a high-altitude regional representative site in the central Himalayas, *J. Geophys. Res.-Atmos.*, 119, 1592–1611, <https://doi.org/10.1002/2013JD020631>, 2014.
- Shindell, D., Kuylenstierna, J. C. I., Vignati, E., van Dingenen, R., Amann, M., Klimont, Z., Anenberg, S. C., Müller, N., Janssens-Maenhout, G., Raes, F., Schwartz, J., Faluvegi, G., Pozzoli, L., Kupiainen, K., Höglund-Isaksson, L., Emberson, L., Streets, D., Ramanathan, V., Hicks, K., Oanh, N. T. K., Milly, G., Williams, M., Demkine, V., and Fowler, D.: Simultaneously Mitigating Near-Term Climate Change and Improving Human Health and Food Security, *Science*, 335, 183–189, <https://doi.org/10.1126/science.1210026>, 2012.
- Singh, N., Solanki, R., Ojha, N., Janssen, R. H. H., Pozzer, A., and Dhaka, S. K.: Boundary layer evolution over the central Himalayas from radio wind profiler and model simulations, *Atmos. Chem. Phys.*, 16, 10559–10572, <https://doi.org/10.5194/acp-16-10559-2016>, 2016.
- Sinha, P., Sahu, L., Manchanda, R., Sheel, V., Deushi, M., Kajino, M., Schultz, M., Nagendra, N., Kumar, P., Trivedi, D., Koli, S., Peshin, S., Swamy, Y., Tzani, C., and Sreenivasan, S.: Transport of tropospheric and stratospheric ozone over India: Balloon-borne observations and modeling analysis, *Atmos. Environ.*, 131, 228–242, <https://doi.org/10.1016/j.atmosenv.2016.02.001>, 2016.
- Škerlak, B., Sprenger, M., and Wernli, H.: A global climatology of stratosphere–troposphere exchange using the ERA-Interim data set from 1979 to 2011, *Atmos. Chem. Phys.*, 14, 913–937, <https://doi.org/10.5194/acp-14-913-2014>, 2014.
- Škerlak, B., Sprenger, M., Pfahl, S., Tyrlis, E., and Wernli, H.: Tropopause folds in ERA-Interim: Global climatology and relation to extreme weather events, *J. Geophys. Res.-Atmos.*, 120, 4860–4877, <https://doi.org/10.1002/2014JD022787>, 2015.
- Smit, H. G. J., Straeter, W., Johnson, B. J., Oltmans, S. J., Davies, J., Tarasick, D. W., Hoegger, B., Stubi, R., Schmidlin, F. J., Northam, T., Thompson, A. M., Witte, J. C., Boyd, I., and Posny, F.: Assessment of the performance of ECC-ozonesondes under quasi-flight conditions in the environmental simulation chamber: Insights from the Juelich Ozone Sonde Intercomparison Experiment (JOSIE), *J. Geophys. Res.-Atmos.*, 112, d19306, <https://doi.org/10.1029/2006JD007308>, 2007.
- Sprenger, M., Croci Maspoli, M., and Wernli, H.: Tropopause folds and cross-tropopause exchange: A global investigation based upon ECMWF analyses for the time period March 2000 to February 2001, *J. Geophys. Res.-Atmos.*, 108, 8518, <https://doi.org/10.1029/2002JD002587>, 2003.
- Tanimoto, H., Zbinden, R., Thouret, V., and Nédélec, P.: Consistency of tropospheric ozone observations made by different platforms and techniques in the global databases, *Tellus B*, 67, 270703, <https://doi.org/10.3402/tellusb.v67.27073>, 2015.
- Tanimoto, H., Ikeda, K., Okamoto, S., Thouret, V., Emmons, L., Tilmes, S., and Lamarque, J.-F.: Recent changes in the free tropospheric ozone over East Asian Pacific rim, International Global Atmospheric Chemistry (IGAC) Science Conference, 26–30 September 2016, Breckenridge, CO, USA, 2016.
- Traub, M. and Lelieveld, J.: Cross-tropopause transport over the eastern Mediterranean, *J. Geophys. Res.-Atmos.*, 108, 4712, <https://doi.org/10.1029/2003JD003754>, 2003.
- Trickl, T., Bärtsch-Ritter, N., Eisele, H., Furger, M., Mücke, R., Sprenger, M., and Stohl, A.: High-ozone layers in the middle and upper troposphere above Central Europe: potential import from the stratosphere along the subtropical jet stream, *At-*

- mos. Chem. Phys., 11, 9343–9366, <https://doi.org/10.5194/acp-11-9343-2011>, 2011.
- Tyrlis, E., Škerlak, B., Sprenger, M., Wernli, H., Zittis, G., and Lelieveld, J.: On the linkage between the Asian summer monsoon and tropopause fold activity over the eastern Mediterranean and the Middle East, *J. Geophys. Res.-Atmos.*, 119, 3202–3221, <https://doi.org/10.1002/2013JD021113>, 2014.
- Varotsos, C., Kalabokas, P., and Chronopoulos, G.: Association of the Laminated Vertical Ozone Structure with the Lower-Stratospheric Circulation, *J. Appl. Meteorol.*, 33, 473–476, 1994.
- Venkat Ratnam, M., Ravindra Babu, S., Das, S. S., Basha, G., Krishnamurthy, B. V., and Venkateswararao, B.: Effect of tropical cyclones on the stratosphere–troposphere exchange observed using satellite observations over the north Indian Ocean, *Atmos. Chem. Phys.*, 16, 8581–8591, <https://doi.org/10.5194/acp-16-8581-2016>, 2016.